Effective volume of supernovae samples and sample variance

Zhongxu Zhai,[1,2,3,4,*] Will J. Percival,[3,4,†] and Zhejie Ding[1,2]

[1]Department of Astronomy, School of Physics and Astronomy, Shanghai Jiao Tong University, Shanghai 200240, China
[2]Shanghai Key Laboratory for Particle Physics and Cosmology, Shanghai 200240, China
[3]Waterloo Center for Astrophysics, University of Waterloo, Waterloo, Ontario N2L 3G1, Canada
[4]Department of Physics and Astronomy, University of Waterloo, Waterloo, Ontario N2L 3G1, Canada

(Received 10 March 2023; accepted 26 February 2024; published 14 March 2024)

The source of the tension between local Supernova (SN) Ia based Hubble constant measurements and those from the cosmic microwave background or (baryon acoustic oscillation+big bang nucleosynthesis) measurements is one of the most interesting unknowns of modern cosmology. Sample variance forms a key component of the error on the local measurements, and will dominate the error budget in the future as more SNe Ia are observed. Many methods have been proposed to estimate sample variance in many contexts, and we compared results from a number of approximate methods to estimates from N-body simulations in a previous paper, confirming that sample variance for the Pantheon SNe Ia sample does not solve the Hubble tension. We now extend this analysis to include the more accurate analytic method based on calculating correlations between the radial peculiar velocities of SNe Ia, comparing this technique with results from numerical simulations. We consider the dependence of these errors on the linear power spectrum and how nonlinear velocities contribute to the error. Using this technique, and matching sample variance errors from more approximate methods, we can define an effective volume for SNe Ia samples, finding that the Pantheon sample is equivalent to a top-hat sphere of radius $\sim 220\ h^{-1}$ Mpc. We use this link between sample-variance errors to compute ΔH_0 for idealized surveys with particular angular distributions of SNe Ia. For example, a half-sky survey at the Pantheon depth has the potential to suppress the sample variance of H_0 to ~ 0.1 km s^{-1} Mpc^{-1}, a significant improvement compared with the current result. Finally, we consider the strength of large-scale velocity power spectrum required to explain the Hubble tension using sample variance, finding it requires an extreme model well beyond that allowed by other observations.

DOI: 10.1103/PhysRevD.109.063519

I. INTRODUCTION

The determination of the Hubble constant using the local distance ladder relies on a sample of type Ia Supernovae (SNe Ia) with high quality [1,2]. Since each SN Ia observation probes the space-time along the line of sight (LoS), inhomogeneities between the observer and the SN Ia alter the value of H_0 recovered. For a set of SNe Ia, these distortions introduce sample variance in the final measurement of H_0. This effect can be reduced when we increase the number of SN Ia observations in different directions. Instead of considering individual LoS, we can take a holistic view considering that the SNe Ia cover a patch in the Universe, and that this patch does not follow the behavior of the background. By considering density fluctuations on scales larger than the patch, we can calculate the expected variance of parameters such as H_0 between a set of patches. These methods—looking at perturbations along each line-of-sight or looking at perturbations in patches of the universe—were compared in an earlier paper [3] and shown to give consistent results. When the current compilation of SNe Ia is taken into account, we found that the sample variance error is around ~ 0.4 km s^{-1} Mpc^{-1}, not able to explain the tension of H_0 using local distance ladder and cosmic microwave background, as has been found previously [4–10].

Although the amplitude of sample variance is not sufficient to explain the Hubble tension, it still contributes a significant component of the error budget of the H_0 determination, given the fact that the latest measurement has reached a combined uncertainty level of 1 km s^{-1} Mpc^{-1}. All methods for calculating sample variance start from the same step, integrating the linear power spectrum to quantify the amplitude of density fluctuations. The SNe Ia living in an overdense area experience an additional attraction due to local structures and reduce the H_0 estimate, while the opposite can happen in underdense regions and increase H_0. As discussed above, the behavior of these regions can be

*zhongxuzhai@sjtu.edu.cn
†Also at Perimeter Institute for Theoretical Physics, 31 Caroline St. North, Waterloo, ON N2L 2Y5, Canada.

considered as either giving rise to peculiar velocities of SNe Ia with respect to the background, or changing the cosmology of the overdense/underdense patches such that there are no peculiar velocities within the patch, just each patch of spacetime is behaving in a different way.

The first method considered in [3] (hereafter paper I) was based on how the inhomogeneity δ along the LoS changes the luminosity distance in a frame where the redshift remains constant [11–14]. Relativistic corrections to observations in such a model were considered in [15]. In the local universe, the resulting variance in H_0 can be approximated as $-f\delta/3$ where f is the linear growth rate. The second method considered in paper I was based on methods to determine super sample covariance (SSC) in sets of cosmological simulations [16–18]. Due to the finite volume covered in any simulation, density fluctuations on scales larger than the simulation box give rise to a "DC-level" density fluctuations that is different for each box in a set. This then leads to cosmological parameters that vary between the simulations [17]. The Hubble constant in each box (or patch) is different from the background and measurements within it will give this local value. The third method borrows ideas from the homogeneous top-hat model for structure growth. In a small patch of the universe, the evolution can be governed by the same equations as the background but with a different initial curvature due to perturbations in density. Each sphere is governed by a Friedmann equation with different parameters, leading to a different scale factor inside the patch than the background and thus a different H_0. The fourth method uses numerical simulations directly—in N-body simulations, distances are measured relative to the background, with perturbations resulting in the peculiar velocities that incorporate the dynamics of dark matter.

The three analytical methods described above perturb different parameters in the model: the luminosity distance, cosmological parameters or spatial curvature, with the level of perturbation limited by the density power spectrum. The simulation-based method does not perturb any parameters in the model explicitly, but the correlation of H_0 with the overdensity in the patch δ can be easily computed from the peculiar velocities within the simulation. In this paper, we contrast these methods with a method based on directly modeling the correlations between the radial peculiar velocities of different SNe Ia. In a frame where distances are measured with respect to the background cosmology, and perturbations affect peculiar velocities, the sample variance of H_0 results from the correlated peculiar velocities of the SNe Ia. Such a method was introduced in earlier works [19,20] and has been studied in the constraint on cosmological parameters, see [14,21–29] and references therein. Similar to the nonsimulation methods summarized above and in paper I, the velocity correlation function method can also be classified as an analytical method. However, there are crucial differences. First, this method utilizes the peculiar velocity of the SN Ia directly, which is the source of the sample variance in the H_0 measurement. For methods that perturb parameters, one has to approximate the size and shape of the patch being considered. Instead, by considering the peculiar velocity field directly as defined within a single background cosmology, this method uses the exact geometry of the SN Ia survey. Thus, it provides more accuracy. When originally defined, the method was used to predict the peculiar velocities of dark matter halos leading to results for peculiar velocity surveys and redshift space distortion (RSD) measurements, matching simulation-based analysis. The method gives the effect of sample variance (or RSD) on SN Ia surveys, but the link from peculiar velocity errors to errors on H_0 is not direct—the method to go from the velocity errors to errors on the measurement of H0 requires care, as discussed later, where we use Monte-Carlo simulations to determine this link.

Each of the five methods used to estimate sample variance for SNe Ia measurements provides different insights for the method. By comparing results between direct measurements that include the 3D distribution of SNe Ia and those that approximate this as a simple shape, we can define effective properties of any sample. This effective volume makes it possible to compare and contrast surveys. Ideally, we want to use fast analytic methods to make predictions, but need to do so accurately. The problem with using the analytic methods in paper I directly is that they make too many simplifying assumptions to be accurate. For example, that each SN Ia in the sample has equal weight, and depending on the exact method, they make an approximation such as that the region of influence of every line-of-sight (LOS) to a SN Ia is a sphere entered on the mid-point on the LOS between SN and the observer. However, the SNe Ia at higher redshift have a larger contribution from the Hubble flow than their peculiar velocity, and therefore in terms of the H_0 determination, they should receive more weight. In addition, the sample variance of H_0 is directly affected by the uncertainty of the apparent magnitude of each SN Ia, see, e.g., [7] and thus it is not correct to assume that they are the same given the noise covariance matrix [30].

We therefore need to consider a more realistic method to estimate the effective volume of the SNe sample. By matching the variance ΔH_0 of the approximate methods to a more accurate method, we can achieve this goal and define an effective volume for any sample of SNe Ia in a fast, quantitative, and straightforward way. We could do this calibration using N-body simulations, but this is computationally very expensive. Instead we now show that we can calibrate the fast methods of paper I using the velocity correlation function method. Based on this, we can quickly forecast the sample variance component of ΔH_0 for future SNe Ia surveys as a function of area and number density, and balance the breadth of any survey against density for sample variance errors.

This paper is organized as follows, Sec. II presents the formalism of the radial velocity correlation function. Section III provides the results for the estimate of ΔH_0 and the effective volume of the current SNe data. Section IV includes our discussion and conclusions.

II. VELOCITY CORRELATION FUNCTION

In this section, we briefly review the formalism of the velocity correlation function method developed in the literature, and describe how we apply it to estimate the H_0 variance.

For a set of SNe Ia, the sample variance depends on the relative position of the LoS through the radial velocity correlations, e.g., [14,19,24,28,31]. For example, probing similar LoS multiple times does not reduce the sample variance as much as probing widely separated LoS. In a frame where perturbations manifest as peculiar velocities, the radial velocity correlation function shows how correlated the sample variance errors are between any two SNe Ia.

For multiple SNe Ia we can construct a $n \times n$ matrix, where n is the number of SNe Ia, and each element is the covariance between the radial velocities of two SNe Ia. Given such a matrix, and assuming that the velocities are drawn from a Gaussian distribution, we can easily create Monte-Carlo samples of sets of peculiar velocities. These can then be attached to measured SNe Ia positions and H_0 can be measured for each realization, using the same methodology applied to data. The distribution of H_0 recovered then leads to the sample variance error on H_0. This method can be considered an approximation to N-body simulations, with the simulations evolving the field in order to get the correct nonlinear velocities for the distribution of SNe Ia positions, while the matrix uses a known form for the covariance within a Gaussian random field.

The method starts from the velocity correlation function, which is defined as

$$\Psi_{i,j}(\mathbf{r}) \equiv \langle \mathbf{v}_i(\mathbf{r_a}) \mathbf{v}_j(\mathbf{r_b}) \rangle, \tag{1}$$

where $\mathbf{r} = \mathbf{r_b} - \mathbf{r_a}$ is the separation vector of two host galaxies labeled as "a" and "b", i and j denote the Cartesian components of the velocity and the average is over all the galaxy pairs. In practice, the SN Ia measurements only depend on the radial component of the velocity, and it is convenient to define $\mathbf{u_a} = \hat{\mathbf{r}}_a u_a = \hat{\mathbf{r}}_a (\hat{\mathbf{r}}_a \cdot \mathbf{v_a})$ and $\mathbf{u_b} = \hat{\mathbf{r}}_b u_b = \hat{\mathbf{r}}_b (\hat{\mathbf{r}}_b \cdot \mathbf{v_b})$, where $\hat{\mathbf{r}}$ is the unit direction vector for $\mathbf{r}$.

For a statistically isotropic and homogeneous random vector field, [19] showed that the above velocity correlation tensor can be written as a function of the amplitude of the separation vector $r = |\mathbf{r}|$

$$\Psi_{i,j}(r) = \Psi_{\parallel}(r) \hat{r}_i \hat{r}_j + \Psi_{\perp}(r)(\delta_{ij} - \hat{r}_i \hat{r}_j), \tag{2}$$

the two new functions $\Psi_{\parallel}$, $\Psi_{\perp}$ are the radial and transverse components of the velocity correlation function, respectively. For the radial peculiar velocities, we can write the correlation function as

$$\langle u_a u_b \rangle = \hat{r}_{ai} \hat{r}_{bj} \langle v_i v_j \rangle = \Psi_{\parallel}(r)(\hat{\mathbf{r}}_a \cdot \hat{\mathbf{r}})(\hat{\mathbf{r}}_b \cdot \hat{\mathbf{r}}) \tag{3}$$

$$+ \Psi_{\perp}(r)[\hat{\mathbf{r}}_a \cdot \hat{\mathbf{r}}_b - (\hat{\mathbf{r}}_a \cdot \hat{\mathbf{r}})(\hat{\mathbf{r}}_b \cdot \hat{\mathbf{r}})]. \tag{4}$$

This expression can be further simplified in terms of the angles θ_1 and θ_2 between the separation vector $\mathbf{r}$ and the galaxy position vectors $\mathbf{r_a}$ and $\mathbf{r_b}$, $\cos\theta_a = \hat{\mathbf{r}}_a \cdot \hat{\mathbf{r}}$, $\cos\theta_b = \hat{\mathbf{r}}_b \cdot \hat{\mathbf{r}}$, and $[\hat{\mathbf{r}}_a \cdot \hat{\mathbf{r}}_b - (\hat{\mathbf{r}}_a \cdot \hat{\mathbf{r}})(\hat{\mathbf{r}}_b \cdot \hat{\mathbf{r}})] = \sin\theta_a \sin\theta_b$. In this case, the velocity correlation function is fully determined by the functions $\Psi_{\parallel}$ and $\Psi_{\perp}$. In linear theory, Ref. [22] shows that they can be computed through the power spectrum of the density fluctuation $P(k)$ as follows:

$$\Psi_{\parallel} = \frac{(fH_0)^2}{2\pi^2} \int P(k) \left[j_0(kr) - 2\frac{j_1(kr)}{kr} \right] dk, \tag{5}$$

$$\Psi_{\perp} = \frac{(fH_0)^2}{2\pi^2} \int P(k) \frac{j_1(kr)}{kr} dk, \tag{6}$$

where f is the logarithmic derivative of the linear growth factor with respect to the scale factor and can be approximated as $f \approx \Omega_m^{\gamma}$ with γ as the growth index [32,33], and j_n is the spherical Bessel functions of order n. The power spectrum $P(k)$ can be easily computed using models like the parametrization of [34]. The above equations can determine the velocity correlation function of galaxy pairs. In the limit where $r \to 0$, Eqs. (5) and (6) reduce to the same form, which gives the diagonal elements in the covariance matrix,

$$\sigma_{v_i}^2 = \langle u^2 \rangle = \frac{(fH_0)^2}{6\pi^2} \int P(k) dk, \tag{7}$$

where σ_{v_i} is the dispersion in the peculiar velocities [14]. Thus we have completed the construction of the velocity correlation function for the SNe Ia sample. Note that Eqs. (5)–(7) are only valid for linear scales, where the density-velocity relationship is simple. To extend this into the nonlinear regime, we would need to use the nonlinear velocity power spectrum, rather than scaling the nonlinear density power. For instance, [35] explores the theoretical descriptions for modelling the nonlinear effect on the velocity correlation function in redshift space. Although our linear model is clearly too simple, the results given below show good agreement with the simulation-based analysis. The velocity correlation function method has been previously used to predict errors for a SN Ia sample. For instance, [36] adopt a likelihood analysis to search the significance of

the bulk velocity using the JLA sample at low redshift. And [37] uses the same SNe Ia sample to retrieve constraint on the growth-related cosmological parameters using SN peculiar velocity with and without combining the weak lensing signal. We extend this work, comparing the correlation function method to approximate methods and simulations, and using the comparison to define the effective volume of a SN sample. Using this effective volume we can easily make predictions for future projects that would otherwise be computationally prohibitive.

III. RESULTS

In this section, we use the velocity correlation function method to estimate the sample variance of H_0 from the current SNe Ia dataset, and investigate extensions including nonlinear corrections to the power spectrum and velocity bias.

A. Estimating the variance of H_0

We compare results from the velocity correlation method against those from numerical simulations calculated using method D in paper I. Our numerical simulation based estimate of the H_0 sample variance relies on a large-scale N-body simulation from UNIT[1] [38]. We use the halo catalog from the simulation, and randomly choose a halo with a mass of $\sim 10^{12-15}\ h^{-1}M_\odot$ as the position of the observer. Then we consider the Pantheon compilation [30] of the SNe Ia sample within the redshift range $0.023 < z < z_{\max}$ where $z_{\max}$ is the maximum redshift in the local distance ladder measurement and the fiducial analysis in [2] adopts $z_{\max} = 0.15$. We assign each SN to the nearest dark matter halo and in this case, the peculiar velocity of the dark matter halo is inherited by the SNe Ia. We can measure H_0 through

$$\log H_0 = 0.2M_B^0 + a_B + 5, \tag{8}$$

where M_B^0 is the fiducial luminosity of SNe Ia and a_B is the expansion parameter describing luminosity distance and redshift relation. The H_0 uncertainty contributed from SNe Ia peculiar velocity is via the uncertainty of

$$\Delta a_B = \frac{1}{N}\sum_{i=1}^{N}\frac{1}{\ln 10}\frac{v_i}{r_i H_0}, \tag{9}$$

where v_i is the peculiar velocity in the radial direction of the ith SN Ia, and N is the total number of SNe Ia used in the analysis [7]. We estimate the final variance ΔH_0 by repeating the process 10^4 times to get a distribution, i.e., each iteration has a different observer in the simulation box and we randomly rotate the SNe Ia sample as a whole into different directions.

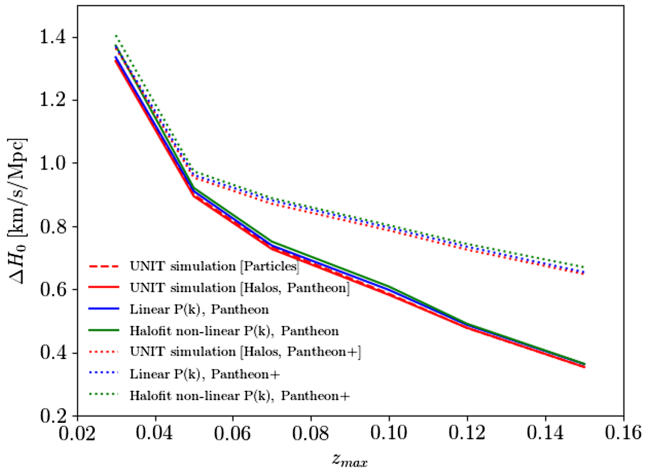

FIG. 1. Variance of H_0 measurements estimated using purely simulation-based method (solid red) and new method based on velocity correlation function (solid blue). For comparison, the dashed red line shows result when the SNe Ia are matched to dark matter particles instead of halos, and the solid green line represents result when the power spectrum for the calculation of velocity correlation function considers nonlinear correction to the density power using halofit, coupled with a linear relationship between density and velocity power spectra.

For our new method based on the velocity correlation matrix, we can use the observed SN Ia positions as the starting point to estimate the velocity covariance matrix. However, in order to utilise the existing routines for analysing simulations, and to compare more closely to the results from N-body simulations, we modify this slightly and apply the same procedure to assign SNe Ia to dark matter halos and then we construct a covariance matrix for peculiar velocities using the formula in Sec. II integrating over the expected power spectrum.[2] The covariance matrix only depends on the relative positions of the SNe Ia (or halos). We then use this covariance matrix to produce a mock data vector for peculiar velocities sampling from a multivariate Gaussian distribution, and assign them to the halos. We repeat this process 10^4 times to estimate ΔH_0.

In Fig. 1, we present ΔH_0 as a function of $z_{\max}$. We can see that our new method of modeling peculiar velocity (solid blue) produces results in excellent agreement with our previous purely simulation-based method (solid red). The relative difference between the two method is no higher than a few percent. They both show a clear

[1] http://www.unitsims.org/.

[2] If, instead, we had used the angular position and redshift of the SNe Ia sample to construct the velocity correlation matrix, this would be kept fixed for all realizations. When we match SNe Ia to the halo catalog, it causes slight variations of the positions in each iteration. Our test shows that the difference of these two methods is less than 5%. We fit to the simulations for both in order to have a cleaner match between the two methods.

monotonic dependence on $z_{\max}$, i.e., higher $z_{\max}$ means more and distant SNe Ia are added in the analysis of distance ladder. For the current fiducial analysis with $z_{\max} = 0.15$, the sample variance of H_0 measurement is lower than $\sim 0.4\ \mathrm{km\,s^{-1}\,Mpc^{-1}}$. The new method further approves the robustness of this estimate and shows that the sample variance itself is not able to fully resolve the tension with Planck.

B. Nonlinear correction

Our model of the velocity correlation function is built upon the linear perturbation theory. A fully nonlinear description requires a model for the nonlinear velocity power spectrum, which may in turn require a detailed analysis using high resolution simulations. However, it is possible to perform a simple approximate analysis using the nonlinear density power spectrum and assuming a linear relationship between density and velocity (such a relationship is often assumed in an analysis of cosmic voids [39]). To do this, we apply the halofit model [40] for nonlinear power spectrum $P(k)$ and redo the estimate of ΔH_0. The result is shown as solid green line in Fig. 1. Since the nonlinear correction can boost the power spectrum at small scales, the immediate impact is to increase the velocity dispersion [Eq. (7)], i.e., the diagonal elements for the covariance matrix, which increases the estimate ΔH_0. However, the comparison with the linear model shows that the impact is quite small and the overall agreement with other methods remains. In addition, one can use models like [35] to describe the nonlinear correction in a more realistic manner, however the agreement between our approach and the simulation-based method seems to show that this effect is negligible for the resulting H_0 variance.

C. Velocity bias

As a byproduct of our analysis for peculiar velocity, we can investigate the large-scale velocity bias—the link between the halo and matter velocity fields—using numerical simulations. Earlier studies have shown that this parameter is close to unity, i.e., the galaxy/halo has a velocity field close to the underlying dark matter field [41–43]. These analyses compare the two-point statistics for galaxies/halos with dark matter particles and explored any dependence of velocity bias on halo mass or redshift.

Our estimate of sample variance for H_0 using numerical simulations can be easily extended to study velocity bias. We replace halos by dark matter particles in the assignment of SNe Ia to halos. In Fig. 1, the dashed red line displays this result. It shows that the two velocity field are exactly the same in terms of ΔH_0, indicating that the velocity bias of dark matter halos is close to unity, similar to the results from literature. The work in [42] shows some deviation of velocity bias from unity at $z = 0$ for small scale, but the deviation is no higher than 5%. Therefore our result is not in significant conflict with theirs, but can serve as an independent measurement of velocity bias.

D. Reanalysis with the Pantheon+ compilation

The results discussed above were based on the Pantheon data, and we note that this catalog was recently updated to Pantheon+, as described in [44], and used to remeasure H_0 in [2]. We now compare the two samples and the sample variance in the new H_0 measurement for Pantheon+. We estimate the sample variance error using the velocity correlation function method, and present the results in Fig. 1, shown as the dotted lines. The first feature is the agreement between the velocity correlation function method and the simulation based method, which matches the agreement found using the Pantheon data. This provides further evidence of the method used in this work. However, there is substantial offset between Pantheon and Pantheon + at higher $z_{\max}$. This is counter-intuitive since Pantheon+ has more SNe Ia than Pantheon. The reason is that Pantheon+ is not a simple extension to Pantheon. The selections and cuts in the new compilation rearrange the catalog significantly, see, e.g., the discussions in [44] and [45]. In the redshift range $0.023 < z < 0.15$ for the H_0 measurement, the overlap between Pantheon and Pantheon+ is less than 50%. More importantly, Pantheon+ has more SNe Ia at low redshift, but fewer at high redshift as shown in Figure 2. The Hubble flow is more significant for individual SN Ia compared with the contribution from peculiar velocity, therefore the high redshift SNe Ia gain more weight in the H_0 determination. At $z > 0.1$, the results from two compilations differ by a factor of two. Although the Pantheon+ has more data, the sample variance in the H_0 measurement is not suppressed. From this point of view, the selection is not optimized, implying that future improvement of the variance could be possible.

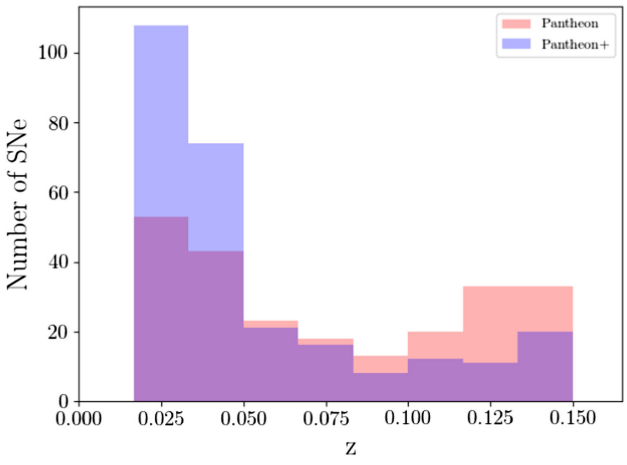

FIG. 2. The redshift distribution of Pantheon and Pantheon+ SNe Ia samples that have been used to measure H_0, in the redshift range $0.023 < z < 0.15$.

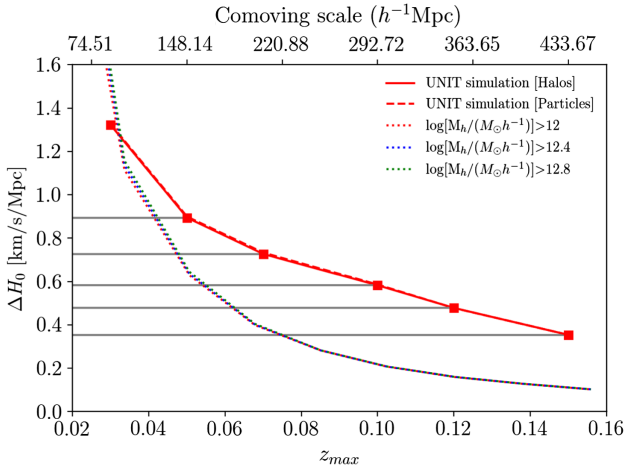

FIG. 3. Estimate of the effective volume of the SNe Ia sample. The solid and dashed red lines represent ΔH_0 when we match SNe Ia to dark matter halos or particles in the UNIT simulation. The dotted lines denote results when we use all halos above some mass cut within some radius to estimate ΔH_0. The interception between the horizontal gray lines and the dotted lines give the effective scale of the SNe Ia sample up to $z_{\max}$.

E. Effective volume of SNe Ia sample

In paper I, we applied a region of influence method and estimated that the SNe Ia sample for the distance ladder measurement only probes a much smaller volume than the maximum redshift $z_{\max} = 0.15$. By comparing techniques for estimating sample variance errors, we can now adopt a straightforward calculation to find the effective region of influence for a SN Ia sample: to do this, we can use all the halos within radius R and estimate ΔH_0 as a function of R. Then we find the scale where the result is the same ΔH_0 as that calculated by the velocity correlation function method. The resultant scale can be considered as the radius of the effective volume that the SNe Ia sample probes.

In Fig. 3, we present the result for the Pantheon sample of SNe Ia. The solid and dashed red lines are the same as Fig. 1, i.e., ΔH_0 from the current Pantheon sample using dark matter halos or particles respectively. The dotted lines stand for the results when we use all halos within some radius. For comparison, we present results with different lower limits of the halo mass. We can see that the result has no dependence on the mass range, matching our previous finding about the velocity bias of dark matter halos. We search the effective volume of the SNe Ia data by matching ΔH_0 of the two measurements, i.e., the horizontal gray lines. For $z_{\max} = 0.15$, we find that the effective volume corresponds to a scale of about 220 h^{-1} Mpc. This is larger than our earlier estimate in [3], meaning that in terms of ΔH_0, the current distance ladder measurement is equivalent to a set of SNe Ia with the same number, within a spherical patch out to redshift ∼0.075. If we look at the Pantheon+ sample, we estimate that the effective volume matches that of a spherical patch out to redshift ∼0.05, smaller than the Pantheon sample since the data is more concentrated at low redshift.

F. Implications for future SNe Ia survey: Ideal case

Although the current error contribution from SNe Ia in the measurement of H_0 is around ∼0.4 km s^{-1} Mpc^{-1}, subdominant in the total error budget, the accuracy will soon be improved with the LSST and Roman surveys [46–48]. Using numerical simulations, we are able to explore the impact of survey designs on the sample variance of the H_0 measurement.

Without any prior knowledge about the survey shape and coverage, we simply assume that the survey is a spherical cap on the sky and the halos are homogeneously distributed within this volume. With this approximation, there are three parameters to define the sample: the survey area A, radius R (sometimes defined using $z_{\max}$), and halo number density n_{sn}. Since the analysis is based on the UNIT simulation, the halo catalog implies an upper limit on the number of objects we can use. For reference, this value is 2.38×10^{-3} [Mpc]$^{-3}$ for dark matter halos within a mass range of $10^{12-15} h^{-1} M_\odot$. We explore the range of n_{sn} that can be as small as 0.1% of this reference number density. For a given R, we define a 2D grid for A and n_{sn}, then we compute ΔH_0 for each A and n_{sn} using halos that can be selected.

As an example, in Fig. 4 we present results for $R = 350$ and $450h^{-1}$ Mpc. The left panel shows the distribution for a range of A and n_{sn}, while the middle and right panels show the dependence on individual parameters. We can see that the overall shape of the curves is similar for different values of R, as well as the change as a function of the parameters. Since the area is proportional to the volume sampled, the decrease of ΔH_0 with A is reasonable. On the other hand, the number density impacts the total number of SNe Ia in a similar manner as the area/volume. Given this dependence, we can perform a simple 2D polynomial fit on the parameters:

$$\Delta H_0 = a_{00} + a_{10}\frac{1}{A} + a_{01}\frac{1}{n_{sn}} + a_{20}\frac{1}{A^2} + a_{11}\frac{1}{An_{sn}} + a_{02}\frac{1}{n_{sn}^2} \tag{10}$$

using the Scikit-learn package [49] and the result is shown as the dotted line in the middle and right-hand side panel of Fig. 4. We can see that the fit is quite a good match to the calculations. In Table I, we summarize the fitting parameters for a few values of R. We note that there is a caveat for the fitting result since, formally, the constant term should vanish when the survey area approaches infinity for any fixed density of SN Ia, but it does not in our fit. The problem is the data we use for the fit is based on noisy measurements, and that we only have data for a physical range of A (less than the full sky). Given the current fitting

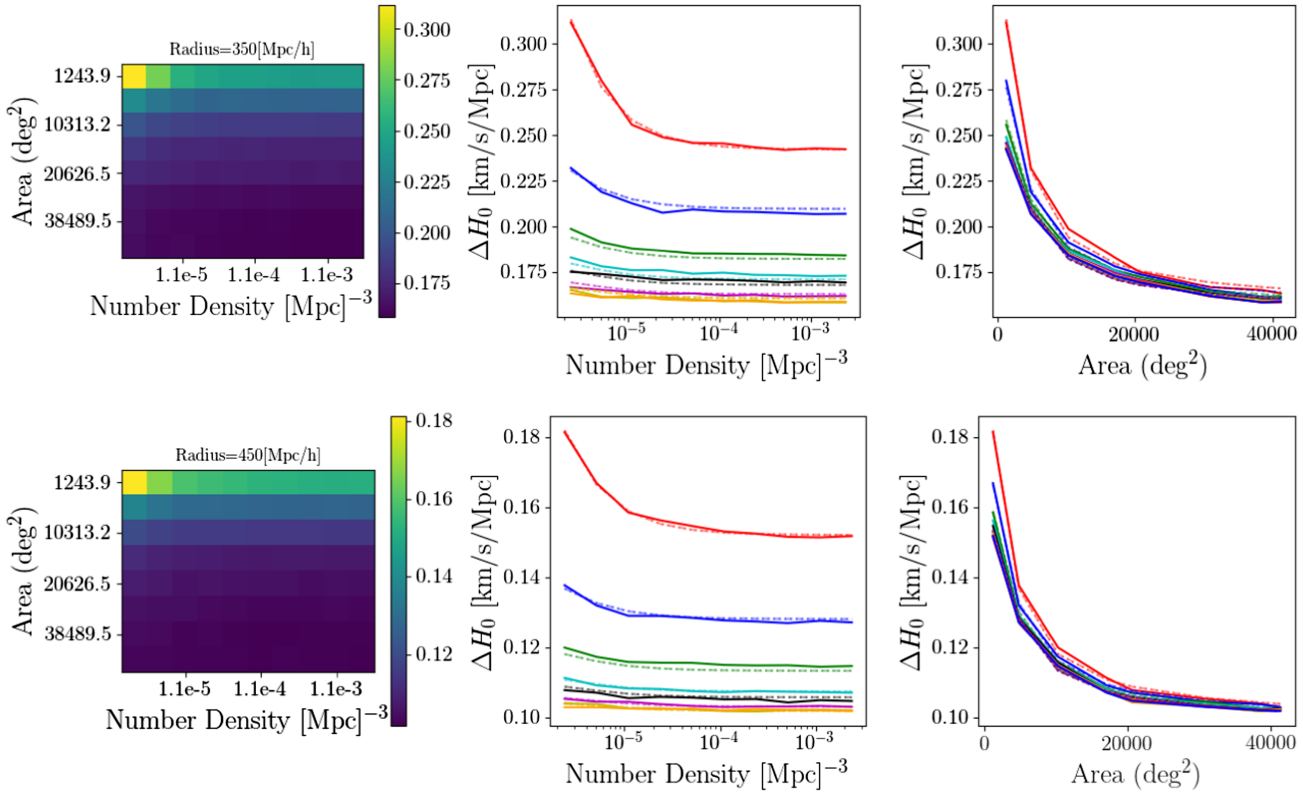

FIG. 4. Dependence of ΔH_0 on the parameters A and n_{sn} assuming an isotropic SNe Ia survey on the sky with an angular coverage of a spherical cap. The left hand panel shows the dependence on the 2D plane, while the middle and right hand panel show the dependence on individual parameters. The different colors in the middle (right) panel shows different values of n_{sn} (A). The dotted lines are the best-fit result with a second polynomial fit [Eq. (10)].

accuracy and the fact that the survey area can never exceed that of the full sky, the current result can be used as a reasonable approximation for practical applications. For an ideal isotropic survey with isotropic coverage in the angular direction, the result can be used to provide a quick estimate for ΔH_0. We note that the coefficients for the second order term are much smaller compared with the first order terms, indicating that a simple volume scaling may already be sufficient for an approximation.

G. Implications for future SN Ia survey: Realistic case

As another example, we can forecast ΔH_0 from future SN observations such as LSST [50], using the distance ladder method. Following [51], we predict the expectation assuming a 5-year LSST SQ survey, which can observe 110k SN events within an angular coverage of 18000 deg^2 and a maximum redshift of 0.35. Since higher redshift may confront redshift evolution and model dependency, the distance ladder usually truncates at, e.g., $z < 0.15$, we also restrict the analysis below this limit. In Fig. 5, we present the expected ΔH_0 as a function of $z_{\max}$. For comparison, we also display the current result from Pantheon compilation. The result shows that a 5 year complete survey may reduce the sample variance of H_0 to ~ 0.1 km s^{-1} Mpc^{-1}, a quarter of the current estimate. In addition, we also fit the LSST result with a simple scaling relation $\Delta H_0 = 0.052/z_{\max} - 0.27$ as shown as the red line in the figure. Note that this fitting relation only uses measurements with redshift below 0.15 and should not extend to higher redshift regimes.

TABLE I. Fitting parameters for the dependence of ΔH_0 on parameters A and n_{sn} using Eq. (10). Parameter A is in unit of deg^2, while n_{sn} is the number density of dark matter halos used in the analysis with a unit of [Mpc]$^{-3}$.

$R[h^{-1}\,\mathrm{Mpc}]$	a_{00}	a_{10}	a_{01}	a_{20}	a_{11}	a_{02}
250	0.27	673	6.15×10^{-8}	-5.72×10^{5}	4.87×10^{-4}	-7.16×10^{-14}
350	0.15	332	1.86×10^{-8}	-2.74×10^{5}	2×10^{-4}	-2.36×10^{-14}
450	0.098	174	7.88×10^{-9}	-1.33×10^{5}	8.44×10^{-5}	-1.14×10^{-14}

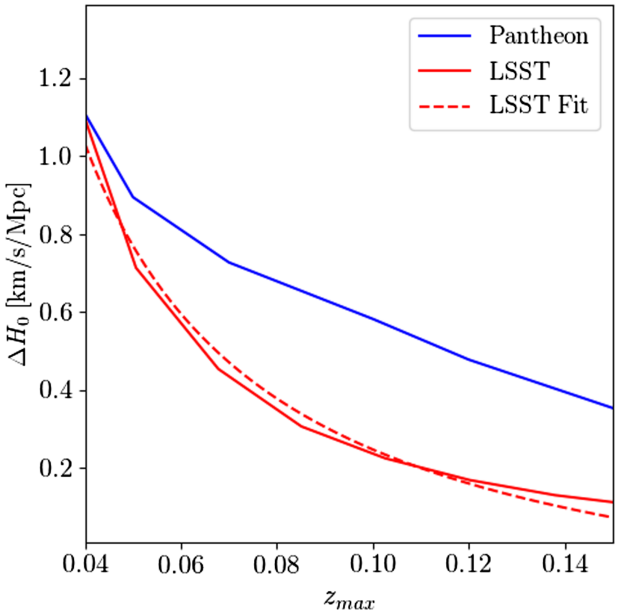

FIG. 5. ΔH_0 forecast based on the LSST SN Ia observations using the UNIT simulation (red solid). We choose a LSST SQ case as detailed in [51] and present the result as a function of $z_{\max}$, the maximum of redshift in the H_0 measurement using the distance ladder. The current result from the Pantheon compilation is also shown (blue solid). The red dashed line shows a simple dependence on $1/z_{\max}$.

H. Large scale modulation

In the velocity correlation function method, as in all of the methods to calculate the sample variance, the matter power spectrum is of critical importance. In particular, increasing the large-scale velocity power spectrum will increase the sample variance. Primordial non-Gaussianity of density perturbations affects the halo mass function and bias on large scale, leaving a k^{-2} divergent signal in the large-scale power spectrum [52–55]. This does not, however, affect the velocity power spectrum as biased objects are expected to still trace the matter velocity field. Another examples of such effect is the curvaton model of the inflationary theory [56,57], which is proposed to explain the hemispherical power asymmetry from cosmic microwave background (CMB) observations [58]. This model introduces a large-amplitude superhorizon perturbation. It is possible that additional models may lead to excess power in the velocity power spectrum, increasing the sample variance.

In order to explore how much extra power is required to increase the sample variance and explain the current Hubble tension, we introduce a toy model to modulate the velocity power spectrum on large scales and investigate the implications on the H_0 sample variance. We multiply the matter power spectrum by a simple function $f = \frac{A}{k} + 1$, where A is a parameter that determines the amplitude of the modulation. The left panel of Fig. 6 shows the power spectrum when we change the value of parameter A. Then we use this modulated power spectrum and redo the calculation of ΔH_0 using the velocity correlation function method as described in previous sections. The resultant ΔH_0 is shown in the right panel of Fig. 6. For comparison, the unmodulated result ($A = 0$) is also shown. Increasing A increases the variance of H_0, as expected given the calculation of velocity correlation function in Sec. II. The horizontal line shows the current H_0 offset of ~5.6 km/s/Mpc between distance ladder and CMB measurements. For mild levels of modulation, ΔH_0 does not increase significantly. For an extreme model with $A = 0.1$ at $z_{\max} = 0.15$, the sample variance ΔH_0 is up to 1.4 km/s/Mpc, comparable and slightly larger than the total error budget using distance ladder. This uncertainty can reduce the H_0 tension below 4σ. However, we should note that such an extreme model is not only modulating

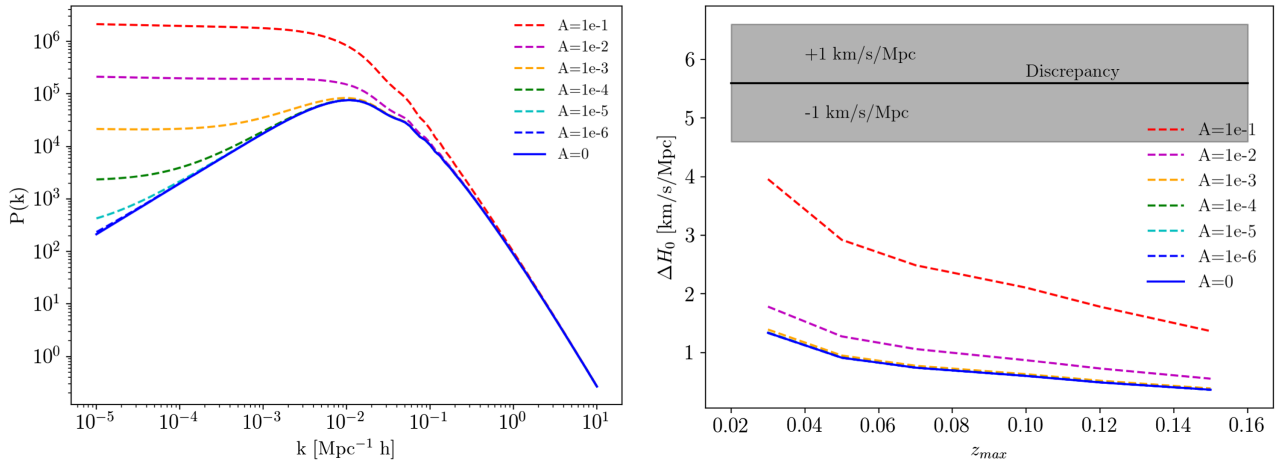

FIG. 6. Left: modulated matter power spectrum with different values of A. This toy model is designed to affect large scale more than small scale. Right: the resultant estimate of ΔH_0 as a function of $z_{\max}$ for different values of A. The horizontal line denotes the current H_0 discrepancy.

the velocity power spectrum at large scale, but changing the whole shape of the velocity power spectrum. Solving the full H_0 tension relying on sample variance and an excess of large-scale power does not look feasible given how much the velocity power spectrum would have to increase, and would produce a tension with other measurements, such as the CMB dipole or RSD for example [59]. We can explicitly test this effect by looking at the velocity dispersion. Given our simple toy model, a large enough ΔH_0 of a few km/s/Mpc to bring the tension within 1σ requires the parameter $A \sim O(1)$. Compared with the unmodulated power spectrum, this boosted model can increase the average amplitude of the peculiar velocity using Eq. (7) from ∼300 km/s to a few thousands km/s, i.e., a boost of roughly a factor of ten. In linear regime, we know that the velocity field is related to the density field via

$$v_r = -\beta \frac{\partial}{\partial r} \nabla_{\mathbf{r}}^2 \delta, \tag{11}$$

where $\nabla_{\mathbf{r}}^2$ is the inverse Laplacian and the subscript "r" denotes the radial direction. If we assume that the underlying density field does not change, the boost of velocity field may purely and linearly come from the structure growth through parameter β. This leads to an increase of the linear growth rate by an order of magnitude, which significantly violates the current observations.

IV. DISCUSSION AND SUMMARY

We have extended our previous (paper I) comparison of methods to estimate the sample variance of H_0 by including an additional method based on the velocity correlation function. In this method, perturbation theory is used to construct a covariance matrix for the radial peculiar velocities of SNe Ia, and realizations are drawn from a mutivariate Gaussian using this matrix. We compare this with a method based on N-body simulations, and find that the replacement of the analytic peculiar velocity correlations with the nonlinear simulation based correlations did not significantly change the estimate of ΔH_0, indicating the robustness of the velocity correlation function using perturbation theory and the dominance of linear scales in the calculation. Given the extra k^2 dependence of the velocity power spectrum compared to that of the density, this is expected. This method allows the sample variance ΔH_0 to be determined without the need for simulations or approximations about the geometry of the survey, such as that it is consistent with a spherical region.

Our analysis using numerical simulations also serves as an independent test for the importance of velocity bias. By selecting halos above some mass scale and compare the results using dark matter particles, we find consistent results showing that velocity bias is very close to unity and not important for such analyses. In addition, we test contributions from nonlinear scale by simply applying a nonlinear correction to the matter power spectrum while keeping the linear relation between density field and velocity field. This is not a full description of nonlinear velocity field, but does show that the nonlinear correction is not significant for the estimate of ΔH_0.

One of the key findings of this paper is to provide a method to determine an effective volume for a set of SNe Ia data, and we apply this to determine the effective volume of the Pantheon SN 1a sample. It is obvious that the volume must be smaller than the maximum redshift of SNe Ia in the sample, since the SN observation only probes the spacetime along the LoS and the density inhomogeneity is not representative of the whole spherical volume defined by the redshift. By comparing methods, we can quantitatively estimate this effective volume by comparing the error contribution to H_0 from the current Pantheon data with a spherical volume of different radii. Our result shows that the current distance ladder measurement is equivalent to a spherical volume with a radius of about 220 h^{-1} Mpc, roughly half the distance to $z = 0.15$. When we investigate the locally perturbed background within a cosmological model such as the Lemaitre-Tolman-Bondi (LTB) model, one needs to be careful about the volume or scales that the SNe Ia data can actually sample. In terms of the H_0 uncertainty itself, our estimate of the sample variance is consistent with the LTB or void-based analysis that they are not able to resolve the tension, see, e.g., [60,61].

Given the estimate of ΔH_0 made using the velocity correlation function method, we can anticipate how the uncertainty of H_0 is affected by the volume covered, total number, or distribution of the SNe Ia. Using the simulated halo catalog, we study the dependence of ΔH_0 on the volume and number density of SNe Ia. In this case, the sample variance is purely from peculiar velocity and we find a clear dependence on the volume and number density. We consider a possible future SNe Ia survey with isotropic distribution and fit the dependence on volume and number density with a second order polynomial model allowing fast calculations. We find that ΔH_0 is more sensitive to the total area than number density: as SNe Ia surveys become sample variance limited covering a wide angular regions will become important. With a half-sky survey, or LSST-like survey in the future, we can expect that the sample variance of H_0 will decrease to 0.1 km s^{-1} Mpc^{-1}, a significant improvement compared with the latest measurement.

Within the framework of the velocity correlation function method, we can additionally investigate the impact of boosting the velocity power spectrum at large scales. We apply a simple toy model to modulate the power spectrum at large scales. As expected, the boost of large scale power can increase the final estimate of the H_0 sample variance. However, to mitigate or solve the tension, it requires an extreme model which may beyond the parameter space allowed by the current observational data. This analysis further demonstrates the severity of the current H_0 tension.

ACKNOWLEDGMENTS

We thank the anonymous reviewers for their careful reading of our manuscript and their many insightful comments and suggestions that have significantly improved this paper. Research at Perimeter Institute is supported in part by the Government of Canada through the Department of Innovation, Science and Economic Development Canada and by the Province of Ontario through the Ministry of Colleges and Universities. Z. Z. is supported by NSFC (12373003), the National Key&D Program of China (2023YFA1605600), and acknowledges the generous sponsorship from Yangyang Development Fund. Z. D. is supported by NSFC (12273020) and National Key R&D Program of China (2023YFA1607800, 2023YFA1607802). This research was enabled in part by support provided by Compute Ontario [62]and the Digital Research Alliance of Canada [63].

[1] A. G. Riess, L. M. Macri, S. L. Hoffmann, D. Scolnic, S. Casertano, A. V. Filippenko, B. E. Tucker, M. J. Reid, D. O. Jones, J. M. Silverman, R. Chornock, P. Challis, W. Yuan, P. J. Brown, and R. J. Foley, Astrophys. J. **826**, 56 (2016).
[2] A. G. Riess, W. Yuan, L. M. Macri, D. Scolnic, D. Brout, S. Casertano, D. O. Jones, Y. Murakami, L. Breuval, T. G. Brink, A. V. Filippenko, S. Hoffmann, S. W. Jha, W. D. Kenworthy, J. Mackenty, B. E. Stahl, and W. Zheng, Astrophys. J. Lett. **934**, L7 (2022).
[3] Z. Zhai and W. J. Percival, Phys. Rev. D **106**, 103527 (2022).
[4] V. Marra, L. Amendola, I. Sawicki, and W. Valkenburg, Phys. Rev. Lett. **110**, 241305 (2013).
[5] R. Wojtak, A. Knebe, W. A. Watson, I. T. Iliev, S. Heß, D. Rapetti, G. Yepes, and S. Gottlöber, Mon. Not. R. Astron. Soc. **438**, 1805 (2014).
[6] A. Enea Romano, Int. J. Mod. Phys. D **27**, 1850102 (2018).
[7] H.-Y. Wu and D. Huterer, Mon. Not. R. Astron. Soc. **471**, 4946 (2017).
[8] D. Camarena and V. Marra, Phys. Rev. D **98**, 023537 (2018).
[9] M. G. Dainotti, B. De Simone, T. Schiavone, G. Montani, E. Rinaldi, and G. Lambiase, Astrophys. J. **912**, 150 (2021).
[10] M. G. Dainotti, B. D. De Simone, T. Schiavone, G. Montani, E. Rinaldi, G. Lambiase, M. Bogdan, and S. Ugale, Galaxies **10**, 24 (2022).
[11] M. Sasaki, Mon. Not. R. Astron. Soc. **228**, 653 (1987).
[12] E. Barausse, S. Matarrese, and A. Riotto, Phys. Rev. D **71**, 063537 (2005).
[13] C. Bonvin, R. Durrer, and M. A. Gasparini, Phys. Rev. D **73**, 023523 (2006).
[14] L. Hui and P. B. Greene, Phys. Rev. D **73**, 123526 (2006).
[15] J. Fonseca, S. Zazzera, T. Baker, and C. Clarkson, J. Cosmol. Astropart. Phys. 08 (2023) 050.
[16] C. S. Frenk, S. D. M. White, M. Davis, and G. Efstathiou, Astrophys. J. **327**, 507 (1988).
[17] E. Sirko, Astrophys. J. **634**, 728 (2005).
[18] T. Baldauf, U. Seljak, L. Senatore, and M. Zaldarriaga, J. Cosmol. Astropart. Phys. 10 (2011) 031.
[19] K. Gorski, Astrophys. J. Lett. **332**, L7 (1988).
[20] K. M. Gorski, M. Davis, M. A. Strauss, S. D. M. White, and A. Yahil, Astrophys. J. **344**, 1 (1989).
[21] A. H. Jaffe and N. Kaiser, Astrophys. J. **455**, 26 (1995).
[22] S. Borgani, L. N. da Costa, I. Zehavi, R. Giovanelli, M. P. Haynes, W. Freudling, G. Wegner, and J. J. Salzer, Astron. J. **119**, 102 (2000).
[23] A. Nusser and M. Davis, Astrophys. J. **736**, 93 (2011).
[24] T. M. Davis, L. Hui, J. A. Frieman, T. Haugbølle, R. Kessler, B. Sinclair, J. Sollerman, B. Bassett, J. Marriner, E. Mörtsell, R. C. Nichol, M. W. Richmond, M. Sako, D. P. Schneider, and M. Smith, Astrophys. J. **741**, 67 (2011).
[25] M. J. Hudson and S. J. Turnbull, Astrophys. J. Lett. **751**, L30 (2012).
[26] T. Okumura, U. Seljak, Z. Vlah, and V. Desjacques, J. Cosmol. Astropart. Phys. 05 (2014) 003.
[27] C. Howlett, L. Staveley-Smith, and C. Blake, Mon. Not. R. Astron. Soc. **464**, 2517 (2017).
[28] Y. Wang, C. Rooney, H. A. Feldman, and R. Watkins, Mon. Not. R. Astron. Soc. **480**, 5332 (2018).
[29] S. S. Boruah, M. J. Hudson, and G. Lavaux, Mon. Not. R. Astron. Soc. **498**, 2703 (2020).
[30] D. M. Scolnic *et al.*, Astrophys. J. **859**, 101 (2018).
[31] Y. Wang, S. Peery, H. A. Feldman, and R. Watkins, Astrophys. J. **918**, 49 (2021).
[32] L. Wang and P. J. Steinhardt, Astrophys. J. **508**, 483 (1998).
[33] A. Lue, R. Scoccimarro, and G. Starkman, Phys. Rev. D **69**, 044005 (2004).
[34] D. J. Eisenstein and W. Hu, Astrophys. J. **496**, 605 (1998).
[35] C. Howlett, Mon. Not. R. Astron. Soc. **487**, 5209 (2019).
[36] D. Huterer, D. L. Shafer, and F. Schmidt, J. Cosmol. Astropart. Phys. 12 (2015) 033.
[37] T. Castro, M. Quartin, and S. Benitez-Herrera, Phys. Dark Universe **13**, 66 (2016).
[38] C.-H. Chuang, G. Yepes, F.-S. Kitaura, M. Pellejero-Ibanez, S. Rodríguez-Torres, Y. Feng, R. B. Metcalf, R. H. Wechsler, C. Zhao, C.-H. To, S. Alam, A. Banerjee, J. DeRose, C. Giocoli, A. Knebe, and G. Reyes, Mon. Not. R. Astron. Soc. **487**, 48 (2019).
[39] A. Woodfinden, S. Nadathur, W. J. Percival, S. Radinovic, E. Massara, and H. A. Winther, Mon. Not. R. Astron. Soc. **516**, 4307 (2022).
[40] R. Takahashi, M. Sato, T. Nishimichi, A. Taruya, and M. Oguri, Astrophys. J. **761**, 152 (2012).

[41] V. Desjacques and R. K. Sheth, Phys. Rev. D **81**, 023526 (2010).
[42] J. Chen, P. Zhang, Y. Zheng, Y. Yu, and Y. Jing, Astrophys. J. **861**, 58 (2018).
[43] P. Zhang, Astrophys. J. **869**, 74 (2018).
[44] D. Scolnic *et al.*, Astrophys. J. **938**, 113 (2022).
[45] A. Carr, T. M. Davis, D. Scolnic, K. Said, D. Brout, E. R. Peterson, and R. Kessler, Pub. Astron. Soc. Aust. **39**, e046 (2022).
[46] S. Dodelson, K. Heitmann, C. Hirata, K. Honscheid, A. Roodman, U. Seljak, A. Slosar, and M. Trodden, arXiv:1604.07626.
[47] V. A. Villar, M. Nicholl, and E. Berger, Astrophys. J. **869**, 166 (2018).
[48] B. M. Rose *et al.*, arXiv:2111.03081.
[49] F. Pedregosa, G. Varoquaux, A. Gramfort, V. Michel, B. Thirion, O. Grisel, M. Blondel, P. Prettenhofer, R. Weiss, V. Dubourg, J. Vanderplas, A. Passos, D. Cournapeau, M. Brucher, M. Perrot, and E. Duchesnay, J. Mach. Learn. Res. **12**, 2825 (2011), https://ui.adsabs.harvard.edu/abs/2011JMLR...12.2825P/abstract.
[50] P. A. Abell *et al.* (LSST Science Collaboration), arXiv:0912.0201.
[51] K. Garcia, M. Quartin, and B. B. Siffert, Phys. Dark Universe **29**, 100519 (2020).
[52] N. Dalal, O. Doré, D. Huterer, and A. Shirokov, Phys. Rev. D **77**, 123514 (2008).
[53] A. Slosar, C. Hirata, U. Seljak, S. Ho, and N. Padmanabhan, J. Cosmol. Astropart. Phys. 08 (2008) 031.
[54] S. Matarrese and L. Verde, Astrophys. J. Lett. **677**, L77 (2008).
[55] P. Valageas, Astron. Astrophys. **514**, A46 (2010).
[56] A. L. Erickcek, S. M. Carroll, and M. Kamionkowski, Phys. Rev. D **78**, 083012 (2008).
[57] A. L. Erickcek, M. Kamionkowski, and S. M. Carroll, Phys. Rev. D **78**, 123520 (2008).
[58] H. K. Eriksen, F. K. Hansen, A. J. Banday, K. M. Górski, and P. B. Lilje, Astrophys. J. **605**, 14 (2004).
[59] Y. Akrami *et al.* (Planck Collaboration), Astron. Astrophys. **641**, A7 (2020).
[60] D. Camarena, V. Marra, Z. Sakr, and C. Clarkson, Classical Quantum Gravity **39**, 184001 (2022).
[61] D. Huterer and H.-Y. Wu, arXiv:2309.05749.
[62] computeontario.ca.
[63] alliancecan.ca.